Toughening of PA6/EPDM-*g*-MAH/HDPE ternary blends via controlling EPDM-*g*-MAH grafting degree: the role of core–shell particle size and shell thickness

Rui Dou · Yan Zhou · Chao Shen · Lan-peng Li · Bo Yin · Ming-bo Yang

Abstract The formation of core–shell morphology for composite droplet polymer-blend systems containing a polyamide-6 (PA6) matrix, MAH grafted ethylene–propylene–diene rubber (EPDM-*g*-MAH) shell and high-density polyethylene (HDPE) core was studied. Core–shell morphology with various shell thickness of blends was controlled via adding EPDM-*g*-MAH with varying grafting degree. Smaller size of core–shell composite droplets and thicker EPDM-*g*-MAH shell are formed in PA6/EPDM-*g*-MAH/HDPE ternary blends with lower grafting degree of EPDM-*g*-MAH and the corresponding Izod impact strength reaches a optimal value of 35.7 kJ/m^2, which is almost 9–10 times higher than pure PA6 (3.6 kJ/m^2). Further, the toughening mechanism was proposed and the results showed that the thicker EPDM-*g*-MAH shell can better transfer the stress between polymer matrix and dispersed phase particles, resulting in easier fibrillation progress of dispersed phase particles, which absorbs a significant amount of impact energy. However, for the blends with higher grafting degree of EPDM-*g*-MAH, during impact processing the easier deformation of the thinner EPDM-*g*-MAH shell caused overlarge cavitations and naked/debonding fiber or spherical dispersed particles, which reduces the Izod impact strength of blends.

Keywords PA6/EPDM-*g*-MAH/HDPE ternary blends · MAH grafting degree · Core–shell morphology · Toughening

R. Dou · Y. Zhou · C. Shen · L. Li · B. Yin (✉) · M. Yang
State Key Laboratory of Polymer Materials Engineering, College of Polymer Science and
Engineering, Sichuan University, Chengdu 610065 Sichuan, China
e-mail: yinbo@scu.edu.cn

Introduction

Polymer compounding or blending receives increasingly interest because of the relatively easy approach to obtain new polymeric materials with balanced properties. In the past decades, much attention has been devoted to study a pure dispersed phase in matrix system. Recently, important studies were carried out for concerning the controlled change of the phase morphology from classical matrix/dispersed phase system into a composite droplet system for a multiphase polymer blends. Since the mechanical properties of multiphase blends are mainly influenced by phase morphologies and interfacial interaction, it is very important to understand and control the phase morphology of composite droplet in multiphase polymer blends.

In general, for a ternary blends of polymers A, B, and C (A is the continuous matrix; B and C are the dispersed phases), four typical morphology can be obtained: (a) "stacked or acorn formation" of B and C stuck together (b) "capsulation structure" of C encapsulated by B, (c) "capsulation structure" of B encapsulated by C and (d) "isolated formation" of B and C dispersed separately, as shown in Fig. 1. The phase morphology is generally determined by the following factors: interfacial interaction, composition, interfacial tension, viscosity ratio, elasticity, processing parameters, etc. [1]. Tchomakov [2] investigated the effect of PE viscosity, concentration and incorporation sequence on the morphology and mechanical properties of ternary PP/EPDM/PE blends prepared using a twin-screw extruder. Hemmati et al. [3] reported that the composition of components affected only the size of each dispersed phase and had no appreciable effect on the type of morphology. They also reported that systems PP/EPDM or EPR/(HDPE or PS) with an encapsulation type morphology and found that viscosity ratios affected the size of the dispersed phase, but had puny influence on the subinclusion type of morphology [4]. Recently, some research groups have observed the formation of core–shell morphology in ternary polymer blends prepared by melt blending [5–8]. Moreover, Ha et al. [9] reported that, for the ternary blends PP/HDPE/mPE, when the viscosity of mPE is proportionally low, core–shell morphology with mPE fibrils in the shell phase is observed. Jazani et al. [10] discovered that, with decreasing the SEBS/SEBS-g-maleic anhydride (MAH) weight ratio, morphology of PP/PC/SEBS ternary blends changed from the core–shell particles to a mixed of core–shell, rod-like and individual particles.
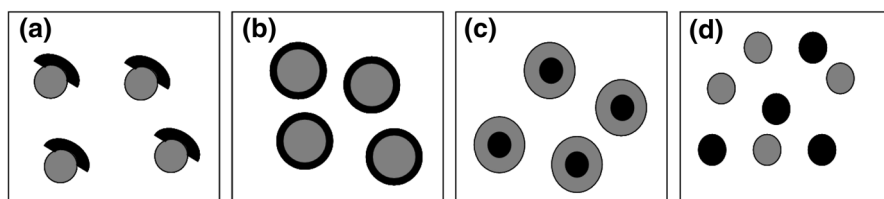
Fig. 1 Some of the most common morphologies observed in ternary blends [40–42]. [Matrix = A; dispersion phases = C (*gray*) and B (*black*)] **a** $\lambda_{B/C} < 0$, $\lambda_{C/B} < 0$, $\lambda_{A/B} > 0$; **b** $\lambda_{B/C} < 0$, $\lambda_{C/B} < 0$, $\lambda_{A/B} < 0$; **c** $\lambda_{B/C} < 0$, $\lambda_{C/B} > 0$, $\lambda_{A/B} < 0$; **d** $\lambda_{B/C} > 0$, $\lambda_{C/B} < 0$, $\lambda_{A/B} < 0$

It is well known that there exists significant correlation between phase morphology and mechanical properties of polymer blends. Involving the properties influenced by phase morphology, tremendous efforts have been paid to revealing the mechanisms responsible for the dramatic toughness increment. Multiple crazing [11–13], shear yielding [11, 12, 14–16], crazing with shear yielding [17, 18], rubbery particle stretching and tearing [19, 20] and debonding [12, 15, 16, 21, 22] are the widely accepted toughening mechanisms of polymers [23, 24]. Kim et al. [24] studied micromechanical deformation processes in toughened PP/PA/SEBS-*g*-MA blends prepared by reactive processing, and found that the fibrillated cavitation process resulted in shear yielding of matrix material was triggered by irreversible plastic growth of micro-voids, which is the main energy dissipation during deformation.

In our previous work, the formation and evolution of core–shell morphology for PA6/EPDM-*g*-MAH/HDPE ternary blends were investigated from the view of thermodynamic factors, e.g., interfacial tension and kinetic factors, i.e. processing time and processing method [25, 26]. However, most work is qualitative on toughening mechanism while the quantitative relationship between core–shell morphology and property has not been established yet so far. Doubtless, a comprehensive understanding of the relation between phase morphology and properties can be very important for us in designing high-performance materials. So, the purpose of this work is to further discuss the effect of core–shell particles size and shell thickness on the mechanical properties for PA6/EPDM-*g*-MAH/HDPE ternary blends, and the different core–shell morphology was designed via controlling the MAH grafting degree of EPDM-*g*-MAH. Also, the toughening mechanism was summarized according to the results of scanning electron microscopy (SEM), double-notch four-point-bend (DN-4-PB) and single-edge-notch three-point-bending (SEN-3PB) tests.

Experimental details

Materials

Polyamide 6 (PA6), with the trademark M2800, was purchased from Guangdong XinHui MeiDa Nylon Company, China (MFR: 4.58 g/10 min at 275 °C and 3.185 N, density: 1.14 g/cm^3 and melting temperature: 225 °C). EPDM, Nordel NDR 4725P, was purchased from Dow Elastomers L.L.C., USA. A commercial HDPE (5000S) with a density of 0.946 g/cm^3 and a melt flow index of 1.0 g/10 min (190 °C, 2.16 kg) was purchased from Lanzhou Petrochemical Company Ltd, China. The DCP peroxide and maleic anhydride (MAH) were all supplied by Ke Long chemical Ltd, Chengdu, China.

Sample preparation

Four kinds of EPDM-*g*-MAH with different MAH grafting degree were prepared by melt extrusion. Firstly, EPDM, MAH and DCP were dried at 80 °C for 6 h in the air oven and were weighted in a certain mass proportion. Subsequently, MAH and DCP

were dissolved in the acetone and then added to the EPDM. After dried at 80 °C for 3 h, the blends were melting extruded by a twin-screw extruder and then pelletized. Five grams of extrudate was heated and dissolved in the 150 ml xylene and then cooled to room temperature. The grafted EPDM was precipitated out and was vacuum filtrated, then washed three times in acetone. The filtered material was dried in vacuum oven at 60 °C for 6 h for Fourier transform infrared spectroscopy (FTIR) tests.

PA6 was dried at 80 °C for 12 h before blending to minimize the effects of moisture. PA6/EPDM-g-MAH/HDPE (70/15/15 wt%) ternary blends were prepared by twin-screw extruder at 240 °C in this study. Then, all blends were injection molded using an injection molding machine (Model: PS40E5ASE, Japan) at 240 °C to obtain standard specimens for mechanical properties testing.

Characterization

Infrared spectroscopy (FTIR)

FTIR spectra were carried out on Nicolet 6700, performing 20 scans, in a range between 550 and 4,000 cm^{-1} with a 4 cm^{-1} resolution. Films of 200–300 µm thickness were prepared by compression molding using a hot press at 170 °C and 5 MPa pressure. The films were vacuum dried at 60 °C for 14 h to evaporate the unreacted MAH.

Measurement of MAH grafting degree

The MAH grafting degree in EPDM-g-MAH was determined by acid–alkali titration method. The sample of 1 g was dissolved in 100 ml xylene at refluxing temperature for half an hour. Then, the hot solution was titrated immediately with 0.1 mol/l KOH/C$_2$H$_5$OH solution, after adding four drops of 1 % phenolphthalein in ethanol as indicator. Titration was stopped when the coloration lasted for 30 s. The sample was completely soluble at the refluxing temperature and did not precipitate during titration. Few drops of water were added to hydrolyze the anhydride group before titration. The equation to calculate the grafting degree of MAH in EPDM-g-MAH can be expressed as follows:

$$\text{Grafting degree (\%)} = \frac{98.06 \times c(V - V_0)}{2 \times 1,000 \times m} \times 100 \qquad (1)$$

where c (mol/l) is the molar concentration of KOH/C$_2$H$_5$OH solution; V_0 (ml) and V (ml) represent volumes of KOH/C$_2$H$_5$OH solution used for titrating pure EPDM and grafted EPDM, respectively; m (g) is the weight of the grafted EPDM; 98.06 (g/mol) is the molecular weight of MAH; and the number 2 represents one anhydride group that would hydrolyze into two carboxylic acid groups after opening up of the anhydride ring. The data presented here were the average of three repeated analysis, and its relative mean deviation was <5 %.

Morphology observations

The morphology of all the samples was characterized by scanning electron microscopy (SEM), FEI-INSPECT F, USA, with an accelerating voltage of 20 kV. The samples were cryo-fractured in liquid nitrogen for SEM analysis, meanwhile the samples were also impact fractured. Before SEM analysis, all the fracture surfaces were gold sputtered before taking images to avoid charge accumulation.

Mechanical testing

Tensile test was performed using an AGS-J testing machine (Shimadzu Corp., Japan) at room temperature according to ASTM D638-10 [27] with a crosshead speed of 50 mm/min. At least seven samples were tested for each reported value. Notched impact strength of the blend was tested with an UJ-40 cantilever beam impact tester (Chengde Jinjian Testing Instrument Co. Ltd., Heibei, China) at room temperature according to ASTM D256-05 [28], and for each sample a gap with the depth of 2 mm was carved through a XQZ-1 gap-sampling machine (Chengde Jinjian Testing Instrument Co. Ltd., Heibei, China). Likewise, at least seven samples were tested for each reported value.

Analysis of the region around the surviving crack tip

Knowledge on the sequence of fracture events is crucial in the fundamental understanding of fracture behavior of polymers. To do so, the double-notch four-point-bending (DN-4PB) test [29–31] was employed to probe the detailed micromechanical deformation of the PA6/EPDM-*g*-MAH/HDPE ternary blends upon fracture. Two nearly identical cracks were cut into the same edge of a rectangular specimen beam. The sharp cracks were generated by a fresh blade which had been chilled in liquid nitrogen and the details of the DN-4PB test specimen are shown in Fig. 2. The DN-4PB tests were performed at room temperature to generate subcritical fracture using an Instron 4302 universal testing machine at a crosshead speed of 5 mm/min. Then, the arrested subcritical crack-tip damage zone from the core region of the sample was isolated, trimmed and thin-sectioned for TOM (Model: Leica DMIP, German). For the TOM study, thin sections of the mid-section with thickness of about 20 μm of the DN-4PB crack-tip damage zone were obtained by sectioning and polishing, following the procedures described by Holik et al. [32]. These thin sections were then investigated using a Leica DMIP optical microscope.

Critical strain energy release rate

A single-edge-notch three-point-bending (SEN-3PB) test was conducted using an AGS-J testing machine and with a clamp length of 40 mm at a crosshead speed of 5 mm/min. The dimensions of specimens are $44 \times 10 \times 4$ mm^3. A typical load–displacement curve of a SENT test for blend was obtained. The critical strain energy release rate (G_c) was determined by the integration of the stress and strain signals
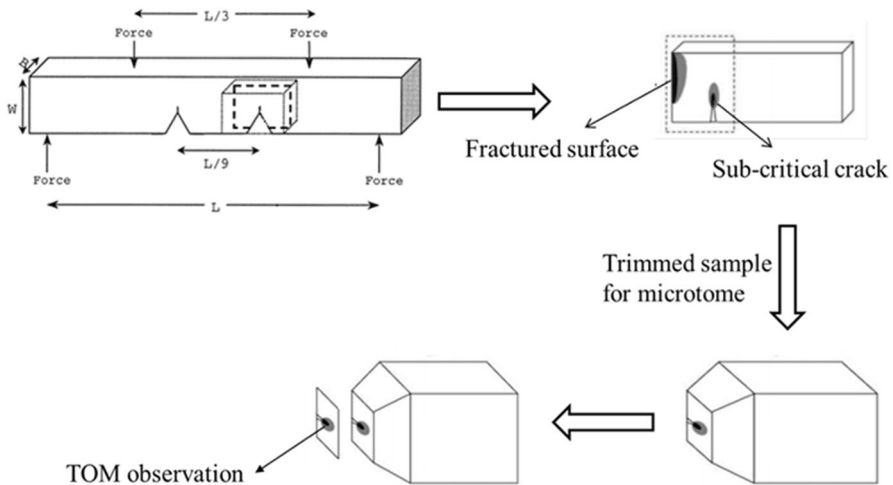
Fig. 2 Schematic illustration of the preparation progress for TOM samples

Fig. 3 Schematic representation of a single-edge notched three-point bend (SEN-3PB) test specimen
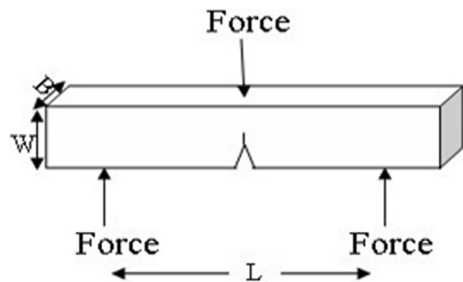

before maximum stress. The details of the SEN-3PB test specimen are shown in Fig. 3.

Results and discussion

FTIR analysis of EPDM-*g*-MAH

Figure 4 shows the FTIR spectra of pure EPDM and EPDM-*g*-MAH prepared by melt mixing. Comparing with the spectra of them, the curves, except for pure EPDM, show two intense absorption bands in the range of 1,710–1,719 cm^{-1} and 1,770–1,792 cm^{-1}, which all corresponds to the C=O symmetric stretching bonds. As has been reported by the literature [33] that the absorption bands in the region of 1,770–1,792 cm^{-1} can be related to grafted anhydride and the absorption band of C=O at 1,713 cm^{-1} is attributed to the presence of dimeric carboxylic acid in EPDM-*g*-MAH, indicating that the MAH has been successfully grafted on EPDM [34]. Further observation shows that from EPDM-*g*-MAH1 to EPDM-*g*-MAH4, the intensity of the absorption peak in 1,713 cm^{-1} is stronger and stronger. Meanwhile,
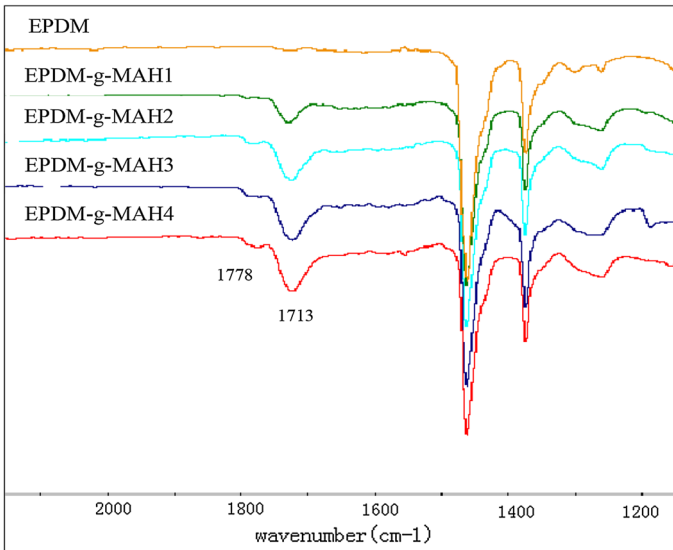
Fig. 4 FTIR spectra of grafted samples

**Table 1** The MAH grafting degree of EPDM-*g*-MAH

Samples	MAH grafting degree (wt%)
EPDM-*g*-MAH1	0.28
EPDM-*g*-MAH2	0.55
EPDM-*g*-MAH3	0.74
EPDM-*g*-MAH4	1.12

combining with the data listed in Table 1, which is calculated by acid–alkali titration method, we can conclude that the MAH grafting degree of EPDM-*g*-MAH gradually increases from EPDM-*g*-MAH1 to EPDM-*g*-MAH4 (0.28, 0.55, 0.74 and 1.12 %, respectively).

Morphology

Figure 5 shows the morphologies of PA6/EPDM-*g*-MAH/HDPE ternary blends with different EPDM-*g*-MAH after selective extraction of EPDM-*g*-MAH minor phase using xylene at 60 °C. Clearly, it can be seen that the morphology consist of PA6 matrix and a composite droplet dispersed phase composed of EPDM-*g*-MAH shell and HDPE core in all PA6/EPDM-*g*-MAH/HDPE ternary blends, which indicates that the MAH grafting degree of EPDM-*g*-MAH has no significant influence on the type of morphology of PA6/EPDM-*g*-MAH/HDPE ternary blends. Further, we can observe that grafting degree of EPDM-*g*-MAH mainly influences the size of core–shell particles and the type of HDPE core. With grafting degree of EPDM-*g*-MAH increasing, the size of composite droplets and the core gradually
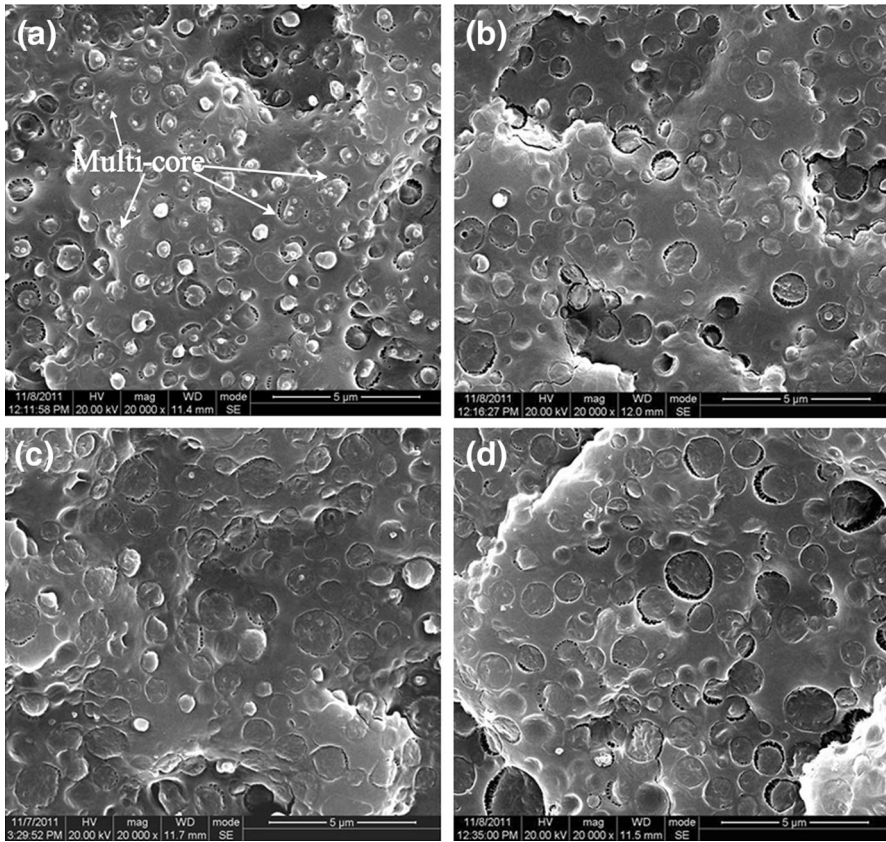
Fig. 5 SEM images of different samples after selective extraction of EPDM-*g*-MAH minor phase using xylene: **a** PA6/EPDM-*g*-MAH1/HDPE, **b** PA6/EPDM-*g*-MAH2/HDPE, **c** PA6/EPDM-*g*-MAH3/HDPE, **d** PA6/EPDM-*g*-MAH4/HDPE

increase. In the ternary blends of PA6/EPDM-*g*-MAH1/HDPE, with low MAH grafting degree of EPDM-*g*-MAH, the average size of core–shell composite droplets is smallest and furthermore, more than one HDPE particles are usually observed inside the EPDM-*g*-MAH domains (shown in Fig. 5a).

To further verify the above results concluded from the SEM photos, the average diameter of composite droplet and the calculated shell thickness are presented in Table 2, using the following equation [35]:

$$H = \frac{1}{2} D_v \left[1 - \sqrt[3]{\left(1 - \phi_{\text{EPDM}-g-\text{MAH/HDPE}} \right)} \right] \tag{2}$$

where D_v is the volume average diameter of the core–shell droplets and $\phi_{\text{EPDM}-g-\text{MAH/HDPE}}$ is the volume faction of EPDM-*g*-MAH based on the dispersed phase. The average diameter of composite droplet D_v increases with increasing MAH grafting degree of EPDM-*g*-MAH, meanwhile the calculated shell thickness

Table 2 Average diameter of composite droplet and the calculated shell thickness of PA6/EPDM-*g*-MAH/HDPE ternary blends

Samples	Average diameter D_υ (μm)	Calculated shell thickness H (μm) using Eq. (2)	Calculated shell thickness H (μm) from Fig. 5
PA6/EPDM-*g*-MAH1/HDPE	0.78	0.078	0.19
PA6/EPDM-*g*-MAH2/HDPE	0.80	0.080	0.072
PA6/EPDM-*g*-MAH3/HDPE	0.96	0.096	0.067
PA6/EPDM-*g*-MAH4/HDPE	0.97	0.097	0.070

H increases slightly from 0.078 to 0.096 μm, which is not in accordance with the actual shell thickness (observed in Fig. 5): the shell thickness in the blends with the lowest MAH grafting degree of EPDM-*g*-MAH has a shell thickness of 0.19 μm which is much thicker than that of the blends with higher grafting degree of EPDM-*g*-MAH (shown in Table 2). This difference can be attributed to the reaction between the carboxyl group in maleic anhydride of EPDM-*g*-MAH and the amino end group of PA6 [36]. On the one hand, the reaction of groups can prevent the diffusion of EPDM-*g*-MAH phase; on the other hand, more grafted copolymer will be formed in the interface between HDPE and EPDM-*g*-MAH. The higher the MAH grafting degree of EPDM-*g*-MAH, the greater the degree of reaction between PA6 matrix and EPDM-*g*-MAH dispersed phase. The molecules' chemical reaction could aggravate the interfacial entanglement of EPDM-*g*-MA and PA6 phase, and subsequently leads to the reduction of chains motion ability. Therefore, it is more difficult for the molecular chain of EPDM-*g*-MAH to migrate to the PA6/HDPE interface, thus reduces the thickness of EPDM-*g*-MAH shell.

Mechanical properties

The ultimate mechanical properties, including the tensile strength, elongation at break and notched impact strength, are shown in Fig. 6. The mechanical property of PA6 matrix was also measured as a reference. Compared with pure PA6, the tensile yield strength of ternary blends decreases, whereas elongation at break increases markedly. However, for the ternary blends, with increasing MAH grafting degree of EPDM-*g*-MAH, the tensile yield strength of ternary blends increases, and elongation at break of ternary blends decreases to some extent, but always far higher than pure PA6 sample. The impact strength of ternary blends of PA6/EPDM-*g*-MAH/HDPE with the presence of core–shell composite droplets shows dramatic increase compared with that of only 3.6 kJ/m^2 for pure PA6. The improvement of impact strength indicates the apparent toughening effect of core–shell structure for PA6. Concerning only the ternary blends, the notched impact strength displays an apparent maximum for the PA6/EPDM-*g*-MAH1/HDPE ternary blends with low MAH grafting degree of EPDM-*g*-MAH. The notched impact strength of PA6/EPDM-*g*-MAH1/HDPE ternary blends is increased up to 35.7 kJ/m^2, which is almost 2–3 times than that of other ternary blends with higher MAH grafting degree
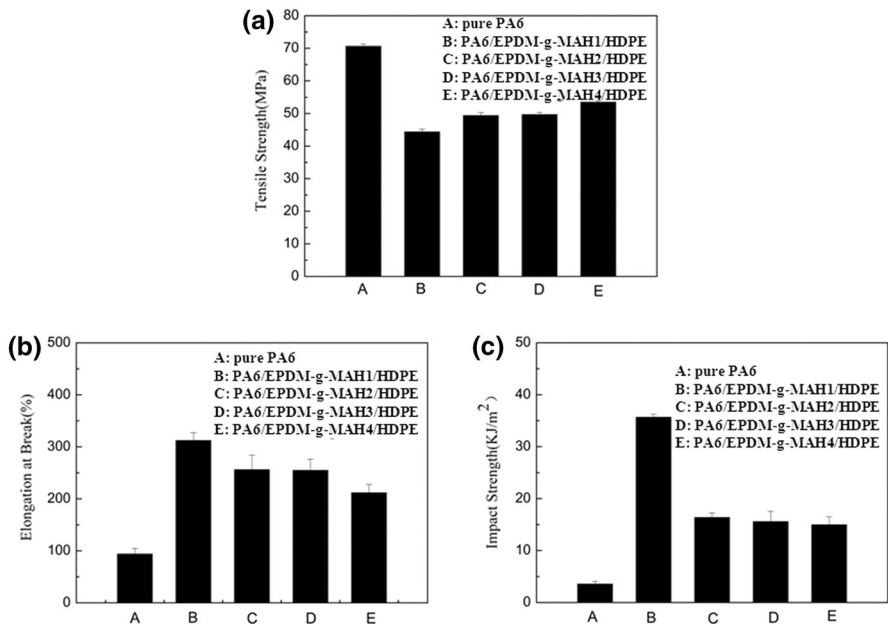
Fig. 6 Tensile strength (**a**), elongation at break (**b**) and impact strength (**c**) of pure PA6 and PA6/EPDM/HDPE ternary blends with different grafting degree of EPDM-*g*-MAH

of EPDM-*g*-MAH and even 9–10 times higher than that of pure PA6, indicating an excellent toughening effect. This reason mainly attributes to the smaller size of core–shell composite droplets and the thickness of EPDM-*g*-MAH shell of PA6/EPDM-*g*-MAH1/HDPE blends. To further clarify the relation between phase morphology and impact properties, the toughening mechanisms of PA6/EPDM-*g*-MAH/HDPE ternary blends with core–shell morphology are investigated below.

Toughening mechanism

SEM analysis of impact fracture surface

The study on the impact-fractured surface morphology is favorable for understanding the toughening mechanism of polymer blends. The fracture surface of a solid polymer material is often an indication of the way of material fractures [37]. As is well known, the fracture process of the specimen under the load of impact includes at least two steps: crack initiation and crack propagation processes [38]. Direct observations on the fracture surfaces obtained from impact tests are shown in Fig. 7 and all SEM graphs correspond to the back of crack-initiation region. For PA6/EPDM-*g*-MAH/HDPE ternary blends, the micro-morphology of fracture surface demonstrates that intensive yielding deformation and extensive plastic flow of the PA6 matrix occurred during the Izod impact process, thereby dissipating a significant amount of impact energy. For the PA6/EPDM-*g*-MAH/HDPE ternary
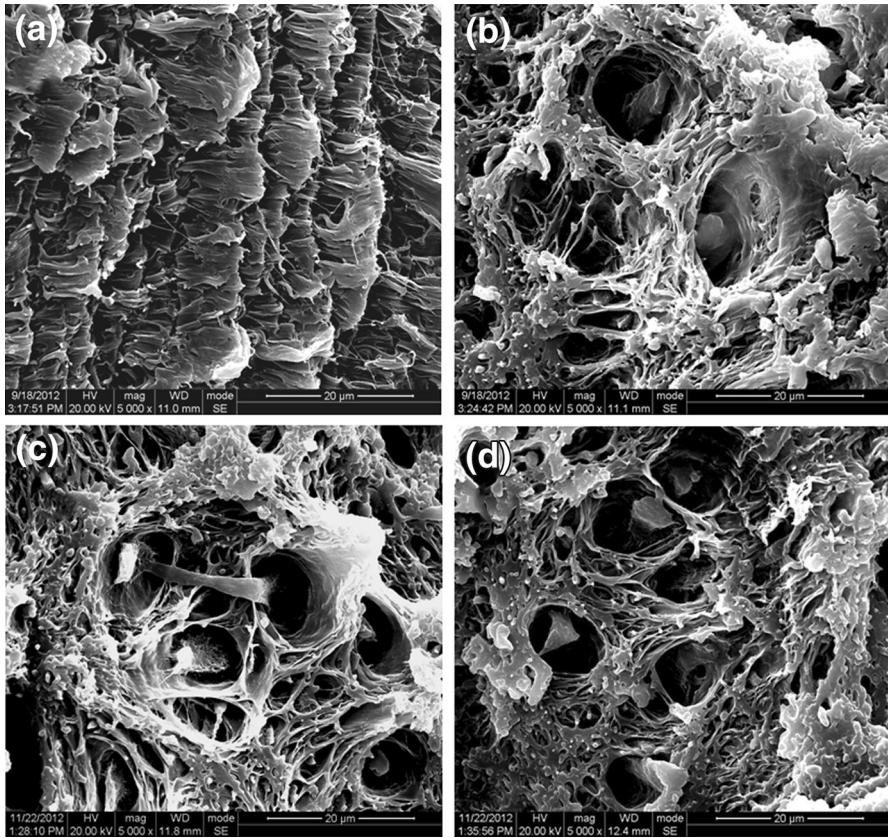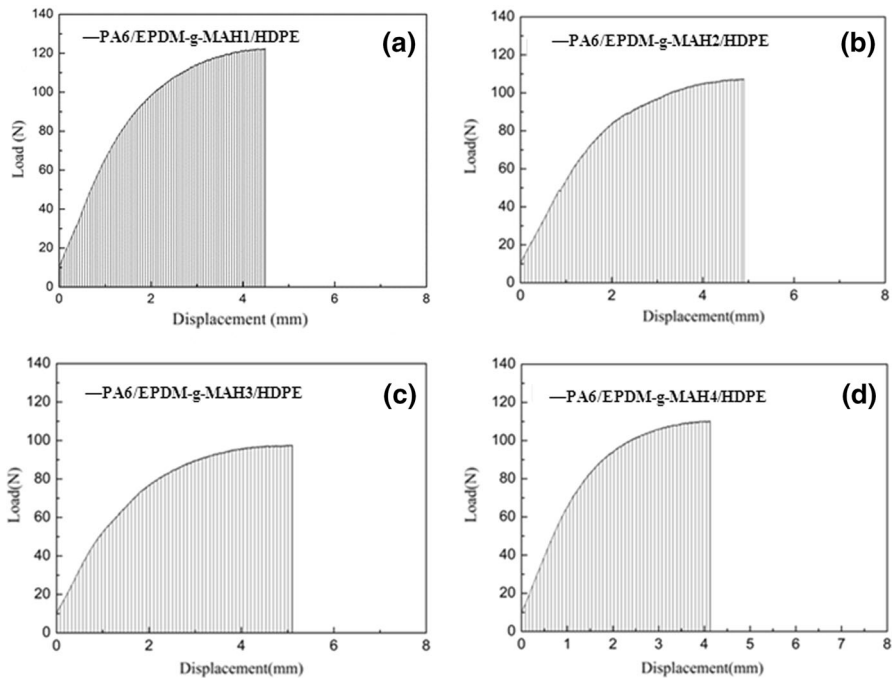
Fig. 7 SEM images of impacted surface of different samples. **a** PA6/EPDM-*g*-MAH1/HDPE, **b** PA6/EPDM-*g*-MAH2/HDPE, **c** PA6/EPDM-*g*-MAH3/HDPE, **d** PA6/EPDM-*g*-MAH4/HDPE

blends with higher MAH grafting degree of EPDM-*g*-MAH (Fig. 7b–d), it is observed that matrix shear yielding takes place but the fracture surfaces generate over large cavitations and naked/debonding fiber or spherical dispersed particles. These cavitations and naked/debonding fiber or spherical dispersed particles are caused by the deformation of EPDM-*g*-MAH rubber and the tensile deformation of core–shell particles during the Izod impact process, separately. This suggests that notched impact strength of these three kinds of blends would not be improved greatly. But it can be observed that intensive yielding deformation of PA6 matrix occurred, elongated core–shell particles and the fibrils caused by the tensile deformation of EPDM-*g*-MAH shell between dispersed phase particle and matrix during Izod impact text. This suggests that notched impact strength of blends would be improved to a limited extent. However, extensive shear yielding, plastic deformation and a large amount of fibrillar structure can be seen throughout the entire region in the PA6/EPDM-*g*-MAH1/HDPE ternary blends with low MAH grafting degree of EPDM-*g*-MAH, as shown in Fig. 7a. Most of all, plastic

deformation zone in the fracture surface can be observed, but no cavitation and naked/debonding fiber or spherical dispersed particles can be found. Therefore, it can be concluded that the core/shell dispersed particles can avoid the rupture of themselves under tensile stress, and thicker EPDM-g-MA shell can prevent debonding from occurring, ensure stress transfer between dispersed particles and polymer matrix. Thus, the fibrillation progress of core–shell dispersed particles without overlarge defect can absorb plenty of fracture energy and improve greatly the notched Izod impact strength of PA6/EPDM-g-MAH1/HDPE ternary blends, which is consistent with the results shown in Fig. 6c.

Critical strain energy release rate

Figure 8 shows the load–displacement curves of SENT tests for PA6/EPDM-g-MAH/HDPE ternary blends. The crack-initiation energy (G_c, critical strain energy release rate) was determined by the integration of the stress and strain signals before maximum stress. Critical strain energy release rate (G_c) obtained from single-edge single-notched three-point-bending measurement of different PA6/EPDM-g-MAH/HDPE specimens is summarized in Table 3. The critical strain energy release rate (G_c) decreases with increasing MAH grafting degree of EPDM-g-MAH. The value

Fig. 8 Load–displacement curves of SENT tests for PA6/EPDM-g-MAH/HDPE ternary blends: **a** PA6/EPDM-g-MAH1/HDPE, **b** PA6/EPDM-g-MAH2/HDPE, **c** PA6/EPDM-g-MAH3/HDPE, **d** PA6/EPDM-g-MAH4/HDPE

Table 3 Critical strain energy release rate (G_c) obtained from single-edge single-notched three-point bending measurement of different PA6/EPDM-g-MAH/HDPE specimens

Samples	G_c (J)
PA6/EPDM-g-MAH1/HDPE	0.407
PA6/EPDM-g-MAH2/HDPE	0.391
PA6/EPDM-g-MAH3/HDPE	0.381
PA6/EPDM-g-MAH4/HDPE	0.344

of G_c displays an apparent maximum 0.407 J in the PA6/EPDM-g-MAH1/HDPE ternary blends with low MAH grafting degree of EPDM-g-MAH, which illustrates stronger resistance of crack propagation.

Analysis of the damage zone around the surviving crack tip

The crack-initiation term of the PA6/EPDM-g-MAH/HDPE ternary blends was also investigated by analyzing the damage zone around the surviving crack tip of the DN-4PB specimens using TOM. The TOM micrographs from the subcritical region of the unbroken notches PA6/EPDM-g-MAH/HDPE ternary blend are shown in Fig. 9. Two important factors should be considered as regards these TOM images: (1) the damage zone size corresponding to the extent of craze growth and (2) the darkness of the damage zone which represents the intensity and number of crazes [39]. It can be clearly seen from Fig. 9 that there exists a certain degree of yield region in all PA6/EPDM-g-MAH/HDPE ternary blends, whereas the propagation distance of crazes in PA6/EPDM-g-MAH1/HDPE (Fig. 9a) with low MAH grafting degree of EPDM-g-MAH is longer than that of the other ternary blends (Fig. 9b–d). In addition, more serious crack propagation and more cracks can be observed in the PA6/EPDM-g-MAH/HDPE ternary blends with higher MAH grafting degree of EPDM-g-MAH. In the PA6/EPDM-g-MAH1/HDPE sample, no sign crack propagation can be observed and the cracks have a trend to gather together at the end of the crack tip of cracks. This indicated that the ability to resist crack propagation of PA6/EPDM-g-MAH1/HDPE sample is obviously superior to that of the PA6/EPDM-g-MAH/HDPE ternary blends with higher MAH grafting degree of EPDM-g-MAH. So, fracture toughness PA6/EPDM-g-MAH1/HDPE sample was improved greatly, which is in good accordance with the high notch impact strength.

Structure–property relations

Figure 10 shows the schematic representation of toughening mechanism of PA6/EPDM-g-MAH/HDPE ternary blends. For the blends PA6/EPDM-g-MAH1/HDPE with low MAH grafting degree of EPDM-g-MAH (seen in Fig. 10a), it owns smaller HDPE core and much thicker EPDM-g-MAH shell, which is better to transfer the stress between polymer matrix, meanwhile withstand tensile stress avoid rubber particles to produce cavitations. The
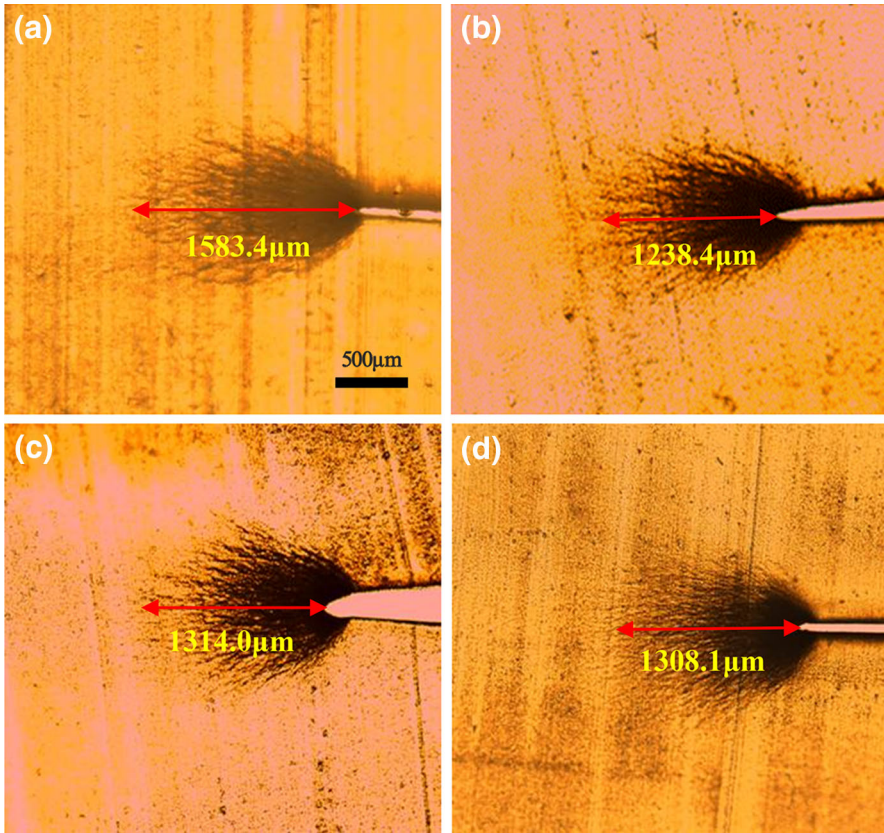
Fig. 9 Bright field TOM photographs of **a** PA6/EPDM-*g*-MAH1/HDPE, **b** PA6/EPDM-*g*-MAH2/HDPE, **c** PA6/EPDM-*g*-MAH3/HDPE, **d** PA6/EPDM-*g*-MAH4/HDPE from the damage zone of the unbroken notch of the DN-4-PB tests

dramatic increase in impact strength is due to the fibrillation progress of the PA6 matrix. While for the blends PA6/EPDM-*g*-MAH/HDPE with higher MAH grafting degree of EPDM-*g*-MAH (seen in Fig. 10b), due to the thinner EPDM-*g*-MAH shell, the interfacial adhesion of PA6/EPDM-*g*-MA interface is relatively poor, hence the fracture surfaces generate overlarge cavitations and naked/debonding fiber or spherical dispersed particles were caused by the deformation of thinner EPDM-*g*-MAH shell and the tensile deformation of core–shell particles.

It is well known that the grafted reaction can be easily controlled in the industrial application, so the core–shell particles with thick EPDM-*g*-MAH shell in our study can be a novel toughening agent to toughen PA6, which will be a practical guidance for the industrial production and application of PA6.
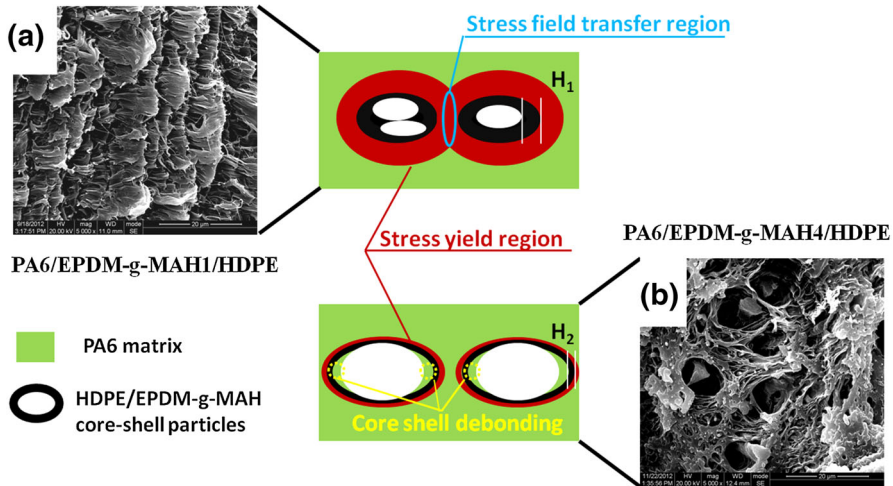
Fig. 10 A sketch showing stress field distribution of PA6/EPDM-*g*-MAH/HDPE blends in different fracture morphologies. **a** PA6/EPDM-*g*-MAH1/HDPE blends, **b** PA6/EPDM-*g*-MAH2/HDPE blends (H_1 and H_2 represent shell thickness: $H_1 > H_2$)

Conclusions

Core–shell particle morphology with different size and different EPDM-*g*-MAH shell thickness was successfully designed via blending EPDM-*g*-MAH with different MAH grafting degree. The smallest core–shell particle size and the thickest shell morphology were obtained when blending the EPDM-*g*-MAH with lowest grafting degree in the PA6/EPDM-*g*-MAH1/HDPE blends. Also, the role of EPDM-*g*-MAH shell thickness in the mechanical properties of the PA6/EPDM-*g*-MAH/HDPE ternary blends has been studied. It was found that with decreasing the shell thickness of EPDM-*g*-MAH, the impact strength of the ternary blends is decreasing, but all better than that of pure PA6. Especially, the blends with the thickest EPDM-*g*-MAH shell, i.e., PA6/EPDM-*g*-MAH1/HDPE, own the optimal impact strength, which is almost 9–10 times higher than pure PA6 and even 2–3 times than the other blends with thinner EPDM-*g*-MAH shell. Meanwhile the toughening mechanisms was confirmed through the method of SEM, DN-4-PB and SEN-3PB and concluded that, for the blends with low MAH grafting degree of EPDM-*g*-MAH, the fibrillation of core–shell particles is formed, which will act as stress transfer layer, resulting in severe shear yielding of matrix; whereas for the ones with higher MAH grafting degree of EPDM-*g*-MAH, the deformation of thinner EPDM-*g*-MAH shell causes overlarge cavitations and fiber or spherical dispersed particles debonding.

References

1. Shirin S, Ahmad A (2009) A review on ternary immiscible polymer blends: morphology and effective parameters. Polym Adv Technol 20:433–447
2. Tchomakov KP, Favis BD, Michel A (2005) Mechanical properties and morphology of ternary PP/EPDM/PE blends. Polym Eng Sci 83:300–309
3. Hemmati M, Nazokdast H, Shariat Panahi H (2001) Study on morphology of ternary polymer blends. II. Effect of composition. J Appl Polym Sci 82:1138–1146
4. Hemmati M, Nazokdast H, Shariat Panahi H (2001) Study on morphology of ternary polymer blends. I. Effects of melt viscosity and interfacial interaction. J Appl Polym Sci 82:1129–1137
5. Luzinov I, Pagnoulle C, Jerome R (2000) Dependence of phase morphology and mechanical properties of PS/SBR/PE ternary blends on composition: transition from core–shell to triple-phase continuity structures. Polymer 41:3381–3389
6. Wilkinson A, Clemens ML, Harding VM (2004) The effects of SEBS-g-maleic anhydride reaction on the morphology and properties of polypropylene/PA6/SEBS ternary blends. Polymer 45:5239–5249
7. Valera TS, Morita AT, Demarquette NR (2006) Study of morphologies of PMMA/PP/PS ternary blends. Macromolecules 39:2663–2675
8. Wang D, Li Y, Xie XM, Guo BH (2011) Compatibilization and morphology development of immiscible ternary polymer blends. Polymer 52:191–200
9. Ha MH, Kim BK, Kim EY (2004) Effects of dispersed phase composition on thermoplastic polyolefins. J App Polym Sci 93:179–188
10. Jazani OM, Arefazar A, Jafari SH (2011) A study on the effects of SEBS-g-MAH on the phase morphology and mechanical properties of polypropylene/polycarbonate/SEBS ternary polymer blends. J App Polym Sci 121:2680–2687
11. Geng CZ, Su JJ, Han SJ, Wang K, Fu Q (2013) Hierarchical structure and unique impact behavior of polypropylene/ethylene–octene copolymer blends as obtained via dynamic packing injection molding. Polymer 54:3392–3401
12. Michler GH (1992) Kunststoff-Mikromechanik: Morphologie, Deformationsund Bruchmechanismen. Hanser, Munich
13. Btinis N, Verdejo R, Cassagnau P, Manchado MAL (2011) Structure and properties of polylactide/natural rubber blends. Mater Chem Phys 129:823–831
14. Dadfar MR, Ghadami F (2013) Effect of rubber modification on fracture toughness properties of glass reinforced hot cured epoxy composites. Mater Des 47:16–20
15. Yin B, Li LP, Zhou Y, Gong L, Yang MB, Xie BH (2013) Largely improved impact toughness of PA6/EPDM-g-MA/HDPE ternary blends: the role of core–shell particles formed in melt processing on preventing micro-crack propagation. Polymer 54:1938–1947
16. Kim GM (1996) Ph.D. Thesis, Martin Luther University, Halle-Wittenberg, Germany
17. Riew CK, Rowe EH, Siebert AR (1976) Toughness and brittleness of plastics. Advances in Chemistry Series, American Chemical Society, Washington, DC. No. 154
18. Lin Y, Chen HB, Chan MC, Wu JS (2008) High impact toughness polypropylene/CaCO$_3$ nanocomposites and the toughening mechanism. Macromolecules 41:9204–9213
19. Gonzalez I, Eguiazabal JI, Nazabal J (2012) Attaining high electrical conductivity and toughness in PA6 by combined addition of MWCNT and rubber. Compos Part A Appl Sci Manuf 43:1482–1489
20. Kinloch AJ, Show SJ, Hunston DL (1983) Deformation and fracture behavior of a rubber-toughened epoxy: 2. Failure criteria. Polymer 24:1355–1363
21. Kinloch AJ, Guild FJ (1996) Predictive modeling of the properties and toughness of rubber-toughened epoxies. In: Riew CK, Kinloch AJ (eds) Toughened plastics II. American Chemical Society, Washington, DC, pp 1–25
22. Dasari A, Zhang QX, Yu ZZ, Mai YW (2010) Toughening polypropylene and its nanocomposites with submicrometer voids. Macromolecules 43:5734–5739
23. Ma LF, Wang WK, Bao RY, Yang W, Xie BH, Yang MB (2013) Toughening of polypropylene with b-nucleated thermoplastic vulcanizates based on polypropylene/ethylene–propylene–diene rubber blends. Mater Des 33:536–543
24. Kim GM, Michler GH, Rosch J (1998) Micromechanical deformation processes in toughened PP/PA/SEBS-g-MA blends prepared by reactive processing. Acta Polym 49:88–95
25. Li LP, Yin B, Zhou Y et al (2012) Characterization of PA6/EPDM-g-MA/HDPE ternary blends: the role of core–shell structure. Polymer 53:3043–3051

26. Dou R, Wang W, Zhou Y, Li LP, Gong L, Yin B, Yang MB (2012) Effect of core–shell morphology evolution on the rheology, crystallization, and mechanical properties of PA6/EPDM-g-MA/HDPE ternary blend. J Appl Polym Sci 129:253–261
27. ASTM D638-10 (1990) Standard test method for tensile properties of plastics. Annual book of ASTM standard, vol 8(1), p 155
28. ASTM D256-05 (1990) Standard test method for impact resistant of plastic and electrical insulation materials. Annual book of ASTM standard, vol 8(1), p 57
29. Hillmyer MA, Bates FS (1996) Synthesis and characterization of model polyalkane–poly(ethylene oxide) block copolymers. Macromolecules 29:6994–7002
30. Sue HJ (1991) Study of rubber-modified brittle epoxy systems. Part I: fracture toughness measurements using the double-notch four-point-bend method. Polym Eng Sci 31:270–274
31. Sue HJ, Yee AF (1993) Study of fracture mechanisms of multiphase polymers using the double-notch four-point-bending method. J Mater Sci 28:2975–2980
32. Holik AS, Kambour RP, Hobbs SY, Fink DG (1979) Microstruct Sci 7:357
33. Grigoryeva OP, Karger-Kocsis J (2000) Melt grafting of maleic anhydride onto an ethylene propylene diene terpolymer (EPDM). Eur Polym J 36:1419–1429
34. Ma LF, Wei XF, Zhang Q, Wang WK, Gu L, Yang W, Xie BH, Yang MB (2012) Toughening of polyamide 6 with β-nucleated thermoplastic vulcanizates based on polypropylene/ethylene–propylene–diene rubber grafted with maleic anhydride blends. Mater Des 33:104–110
35. Reignier J, Favis BD (2000) Control of the subinclusion microstructure in HDPE/PS/PMMA ternary blends. Macromolecules 33:6998–7008
36. Roeder J, Oliveira RVB, Goncalves MC, Soldi V, Pires ATN (2002) Polypropylene/polyamide-6 blends: influence of compatibilizing agent on interface domains. Polym Test 21:815–821
37. Coban O, Bora MO, Sinmazcelik T, Curgul I, Gunay V (2009) Fracture morphology and deformation characteristics of repeatedly impacted thermoplastic matrix composites. Mater Des 30:628–634
38. Yang G, Han L, Haifeng D (2011) Fracture resistance improvement of polypropylene by joint action of core–shell particles and nucleating agent. Mater Sci Eng A Struct 528:1382–1390
39. Afshar A, Massoumi I, Lesan-Khosh R, Bagheri R (2010) Fracture behavior dependence on load-bearing capacity of filler in nano- and microcomposites of polypropylene containing calcium carbonate. Mater Des 31:802–807
40. Ravati R, Favis BD (2010) Morphological states for a ternary polymer blend demonstrating complete wetting. Polymer 51:4547–4561
41. Moini Jazani O, Arefazar A (2011) A study on the effects of SEBS-g-MAH on the phase morphology and mechanical properties of polypropylene/polycarbonate/SEBS ternary polymer blends. J Appl Polym Sci 121:2680–2687
42. Ravati R, Favis BD (2013) Tunable morphologies for ternary blends with poly(butylene succinate): partial and complete wetting phenomena. Polymer 54:3271–3281